THE JOURNAL OF PHYSICAL CHEMISTRY B LETTERS

**2006,** *110,* 10209−10212
Published on Web 05/06/2006

# High-Resolution Electron Tomography Study of an Industrial Ni−Mo/$\gamma$-$Al_2O_3$ Hydrotreating Catalyst

**Krijn P. de Jong,*,† Leon C. A. van den Oetelaar,‡ Eelco T. C. Vogt,‡ Sonja Eijsbouts,‡ Abraham J. Koster,§,|| Heiner Friedrich,† and Petra E. de Jongh†**

*Inorganic Chemistry and Catalysis, Utrecht University, Sorbonnelaan 16, 3584 CA Utrecht, The Netherlands, Hydroprocessing Catalysts Product and Process Research, Research Centre for Catalysts, Albemarle Catalysts Company BV, Amsterdam, The Netherlands, and Molecular Cell Biology, Utrecht University, Padualaan 8, 3584 CA Utrecht, The Netherlands*

*Received: March 14, 2006; In Final Form: April 13, 2006*

The growing demand for high-quality transportation fuels requires their cost-effective production by hydrodesulfurization of crude oils using heterogeneous catalysts. To study the three-dimensional (3D) structure of such a commercial, sulfided Ni−Mo/$\gamma$-$Al_2O_3$ catalyst, electron tomography was applied. The $MoS_2$ particles form an interconnected complex structure within the mesopores of the alumina support. Spatial organization, morphology, and orientation of the $MoS_2$ particles in the pores were resolved with sufficient accuracy to display the 6-Å-spaced $MoS_2$ crystal planes. The proximity of the $MoS_2$ edge planes and more loosely interacting $MoS_2$ basal planes to the alumina support showed the presence of pores smaller than 3 nm, which was confirmed by physisorption experiments. The actual shape of the $MoS_2$ particles cannot be described by simple models as derived from studies on model catalysts. Electron tomography is a unique tool to study the actual 3D structure of complex industrial catalysts with sub-nanometer resolution.

**Introduction.** Oil refining relies on the use of heterogeneous catalysts to deliver high-quality transportation fuels that comply with environmental legislation and address social concerns. In particular, the need for low-sulfur fuels calls for the continuous improvement of hydrotreating catalysts and a better understanding of their properties. Heterogeneous hydrotreating catalysts are composed of a mesoporous alumina support containing a catalytically active phase. The active phase in such catalysts consists of layered $MoS_2$ structures decorated with the promoter (Ni or Co), the so-called Ni−Mo−S or Co−Mo−S phase.[1] The active sites for hydrodesulfurization reactions are associated with sulfur vacancies or metallic character sites at the edges of the $MoS_2$ structures.[2]

Two types of active phases, Type-1 and Type-2, have been described in the literature.[1,3] The active phase of a Type-2 catalyst, as the examined Ni−Mo/$\gamma$-$Al_2O_3$, is characterized by a more complete sulfidation, a weaker interaction between metal sulfides and the alumina support, and a higher intrinsic activity.[1,3a] The morphology of the active phase and its bonding to the alumina support define the extent of the surface area available for hydrodesulfurization reactions. For a detailed account on $MoS_2$ catalysts we refer to relevant reviews.[4]

Transmission electron microscopy (TEM) has become an indispensable technique to obtain detailed structural information on materials. Since the examined volume in TEM is very small compared to the bulk material it is mandatory to complement TEM findings with results from bulk techniques such as nitrogen physisorption, extended X-ray absorption fine structure spectroscopy (EXAFS), or X-ray diffraction (XRD).[4,5] One of the key problems in the characterization of complex porous catalysts by TEM is the projection of three-dimensional (3D) structural information into the image plane. Several authors have pointed out that the distinction between edge and basal bonding of $MoS_2$ stacks on $\gamma$-$Al_2O_3$ is hardly possible from conventional TEM images.[2] In contrast, electron tomography combines multiple images taken at different tilt angles to reconstruct the object's 3D morphology. This approach has been shown to be a versatile method to characterize the 3D structure of biological specimen,[6] quantum dots,[7] and catalysts.[8] For more detailed accounts on the role of electron tomography in catalysis research we refer to the reviews by Anderson, Ziese, or Thomas.[9]

In this paper we report for the first time on the application of high-resolution electron tomography to a complex industrial Ni−Mo/$\gamma$-$Al_2O_3$ catalyst. Key questions in this study are: the 3D spatial organization of the $MoS_2$ particles, the shape of individual $MoS_2$ particles, and the location and orientation of the $MoS_2$ particles with respect to the $\gamma$-$Al_2O_3$ support. In addition we used nitrogen physisorption experiments and XRD measurements to complement and verify our conclusions.

**Experimental Methods.** The commercial Type-2 Ni−Mo /$\gamma$-$Al_2O_3$ (Albemarle Catalysts Company BV) had a metal loading of 2.5 atoms/nm$^2$ for Ni and 8.1 atoms/nm$^2$ for Mo.[10] The catalyst contains also phosphorus, which is a common additive in the preparation of commercial Ni−Mo hydrotreating catalysts. For additional details on catalyst preparation, composition, and $MoS_2$ particles (average length 5.8 nm, average stacking 2.6 layers) we refer to ref 10 (sample ID "NiMo3-T2-G-H"). The

* Author to whom correspondence should be addressed. Phone: +31 30 253 6762. Fax: +31 30 251 1027. E-mail: k.p.deJong@chem.uu.nl.
† Inorganic Chemistry and Catalysis, Utrecht University.
‡ Albemarle Catalysts Company BV.
§ Molecular Cell Biology, Utrecht University.
|| Present address: Leiden University Medical Center, Einthovenweg 20, 2300 RC Leiden, The Netherlands

10.1021/jp061584f CCC: $33.50 

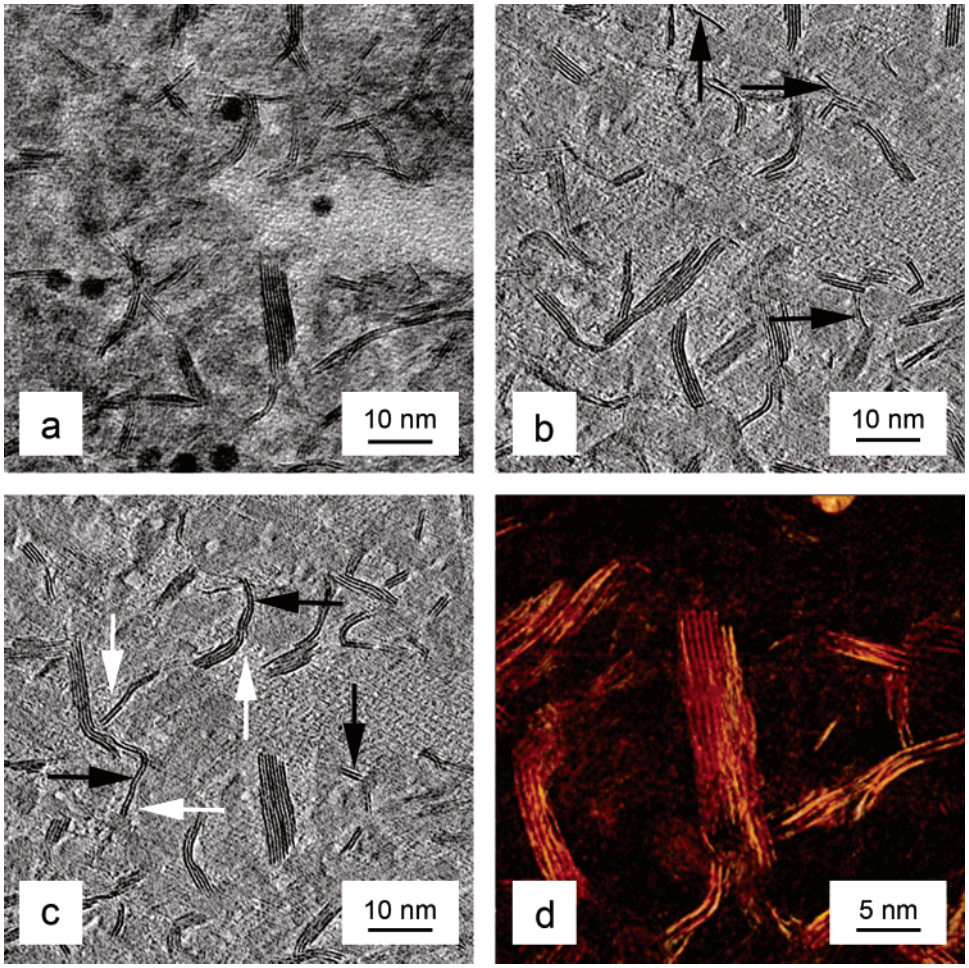


**Figure 1.** TEM image and reconstruction of an epoxy-embedded ultrathin section of the catalyst: (a) image from the tomographic tilt series; (b and c) 5-Å-thick cross-sections through the reconstruction, 6 nm apart. Black arrows indicate $MoS_2$ particles, and white arrows indicate small pores between $MoS_2$ and alumina support. (d) $MoS_2$ particles within a $44 \times 44 \times 32$ nm$^3$ volume visualized without alumina support by volume rendering.

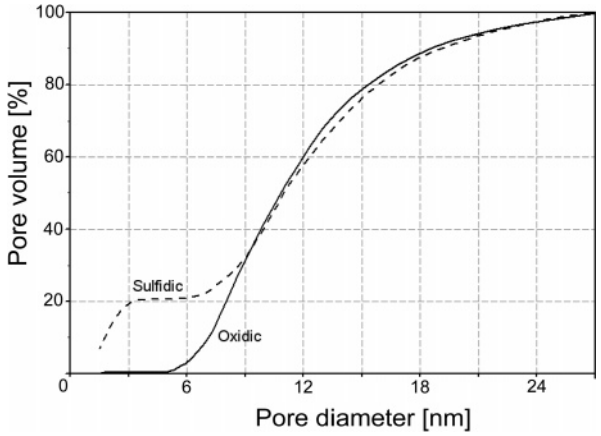


**Figure 2.** Pore-size distributions calculated from the adsorption branches of nitrogen physisorption experiments of the sulfidic catalyst and its corresponding oxidic precursor.

catalyst was sulfided in the gas phase using a mixture of 60 vol % $H_2S$ in $H_2$ at 300 °C for 4 h, cooled to room temperature, and passivated in air. The high $H_2S$ concentration was used to stimulate the formation of $MoS_2$ stacks on catalyst sulfidation. Nitrogen physisorption measurements were performed with Micromeritics (ASAP 2400, Tristar 3000, ASAP 2010) on the sulfidic catalyst and the oxidic precursor. From the adsorption branches of the isotherms pore-size distributions were deduced using the Broekhoff−de Boer formalism.

Extrudates were used in a hydrocracker pretreatment activity test carried out in a trickle flow reactor unit. The feed was coker gas oil, and the reaction conditions were $T = 380$ °C, $p = 100$ bar, liquid hourly space velocity = 2.0/h, $H_2$/oil = 1000 NL/L. These reaction conditions were maintained for a total of 8 days. The extrudates were rinsed in toluene to remove residual oil and powdered in a mortar. After some of the powdered material was embedded in epoxy resin, ultrathin sections (nominally 15-nm-thick) were cut using an ultramicrotome. The sections were then transferred onto a Cu TEM grid. In the last step 5-nm-sized gold colloid particles (Sigma-Aldrich) were applied to the surface of the thin sections to aid in image processing.

Electron microscopy was performed with a Tecnai20 (FEI Company). Bright-field TEM tilt series were recorded at 200 kV using Xplore3D software (FEI) in combination with a bottom-mounted 1k × 1k CCD camera (Gatan GmbH, model 694). The pixel size was 1.7 Å corresponding to a nominal microscope magnification of 100 000×. The tilt series were typically acquired from −70° to +70° with 1° increments. For imaging of the 6 Å features we used an underfocus of a few tens of nanometers. However, when the sample was tilted, areas to the right and left of the rotation axis change their height relative to the focal plane. This change is proportional to the sine of the tilt angle times the distance from the tilt axis, and thus, large focus variations exist between the two extreme sides of the sample. In the presented high-resolution transmission electron microscopy (HRTEM) tilt series the focusing of the area of interest throughout the tilt series was sufficiently accurate

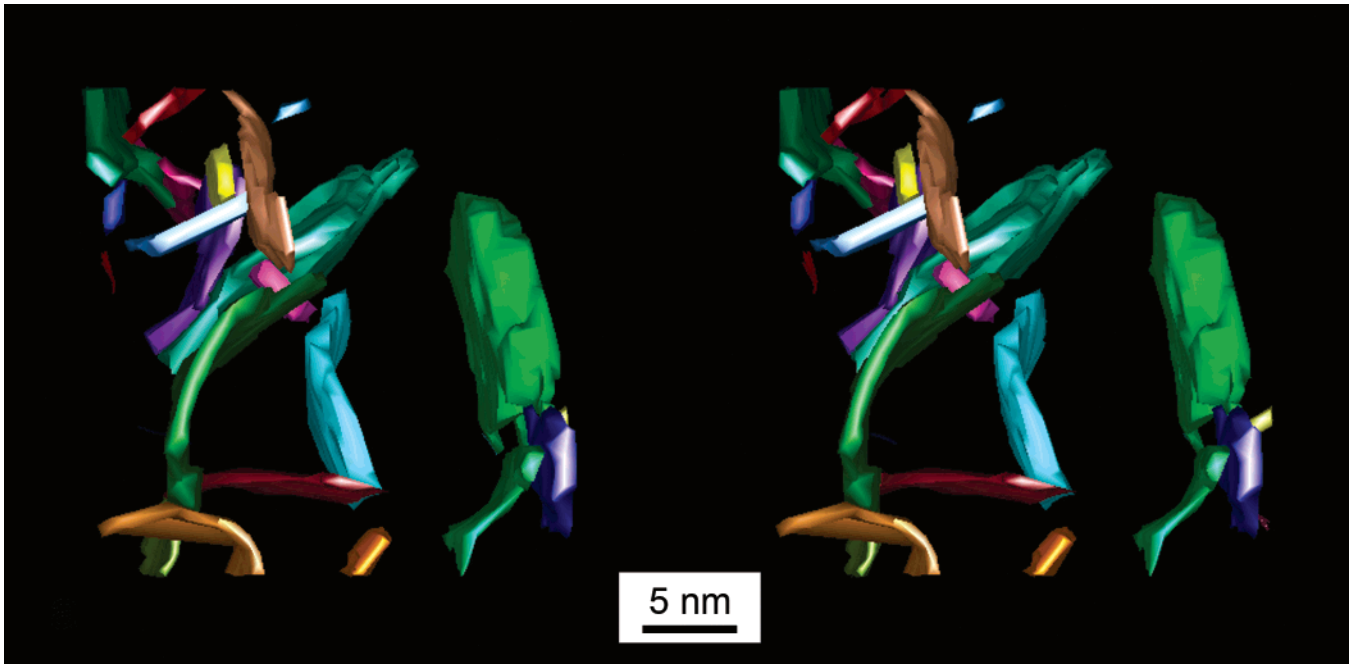


**Figure 3.** Stereoview of interconnected $MoS_2$ particles within a 44 × 44 × 44 $nm^3$ volume of the 3D reconstruction.

to include 126 of the original 141 images for reconstruction of the 3D volume. Images of the tilt series were aligned with respect to a common origin by fiducial markers (colloidal gold particles), and the tomograms then were reconstructed via weighted backprojection in the IMOD program.[11]

**Results and Discussion.** Figure 1a shows an 87 nm × 87 nm HRTEM image of the ultrathin-sectioned epoxy-embedded sulfidic Ni−Mo catalyst. It is a detail from one image of the tomographic tilt series (original size 174 nm × 174 nm × 141 images). Epoxy (bright, granular), alumina support (darker, smooth), and $MoS_2$ crystal planes (dark lines) can be differentiated. The dark circular spots in Figure 1a are 5-nm-sized colloidal gold particles on the surface of the epoxy section that aid in alignment and reconstruction of the tilt series.

Figures 1b and 1c display two 5 Å thin cross-sections through the reconstruction. Again we discern epoxy (granular), alumina support (smooth), and $MoS_2$ crystal planes (dark lines). Even though the spacing between the cross-sections is only 6 nm, Figures 1b and 1c show completely different $MoS_2$ particles. The resolution in the individual cross-sections is sufficient to resolve $MoS_2$ particles (black arrows) consisting of as few as one (Figure 1b) or two crystal planes (Figure 1c). It is immediately apparent that most crystal planes are bent. This bending is displayed in Figure 1d over a 44 × 44 × 32 $nm^3$ volume. Resolving the 6-Å-spaced crystal planes of $MoS_2$ is to the best of our knowledge unprecedented in bright-field (BF) TEM tomography of porous materials.

It must be noted that $MoS_2$ crystal planes oriented parallel to the image plane are not resolved due to limitations in the angular tilt range of the microscope tilt stage. However, most $MoS_2$ crystal planes are viewed in at least some images of the tilt series, and thus the number of resolved crystal planes in a reconstruction is close to the actual number. When looking at Figure 1c it appears as if the bent $MoS_2$ particles are "peeled off" the alumina support, therefore creating small pores (white arrows) and suggesting a loose interaction between both phases. This effect might become more apparent when consulting the movies in the Supporting Information. The contrast between epoxy, alumina support, and $MoS_2$ particles is not sufficient yet to resolve and quantify the pore volume directly from the reconstruction for comparison with physisorption data.

The nitrogen physisorption data in Figure 2 show that pores smaller than 3 nm are created upon sulfidation of the oxidic precursor. The $MoS_2$ particles have grown to occupy a substantial fraction of the available mesopore volume within the alumina support. We found that the Brunauer−Emmett−Teller (BET) surface area increased from 131 $m^2/g$ (oxidic precursor) to 196 $m^2/g$ for the sulfided catalyst. The decrease of the total pore volume from 0.344 mL/g (oxidic) to 0.300 mL/g (sulfidic) nicely coincides with the substantial occupancy of the mesopores by $MoS_2$.

Taking full advantage of the 3D information in the reconstruction as displayed in Figure 1d, we found that most of the $MoS_2$ particles in the investigated area were interconnected in space. In Figure 3 a stereoview of the $MoS_2$ phase within a 44 × 44 × 44 $nm^3$ volume of the 3D reconstruction is displayed. This visualization was created by manually tracing the contours of $MoS_2$ particles in all cross-sections throughout the volume. Separate $MoS_2$ particles consisting of one or more crystal planes are indicated by different colors. It is immediately apparent that the $MoS_2$ particles form a complex structure within the mesoporous alumina support. When looking at the shape of single $MoS_2$ particles it becomes clear that the particles cannot be described by simple models, e.g., triangles or (truncated) hexagons, as derived from studies on model catalysts.[2d,e] X-ray diffraction measurements confirmed deviations from ideal crystalline geometry of $MoS_2$ in the sample.[10] Bending of the crystal planes, as seen in Figures 1 and 3, and the resulting relaxation of the crystal lattice did cause a shift in the position of the (002) diffraction peak from $2\theta = 14.4°$ to 14.0°.[10] This result points to an expansion of the average crystal plane spacing from 6.15 Å to approximately 6.45 Å as bending of the $MoS_2$ crystal planes causes a lattice mismatch in a fashion similar to the one observed for turbostratic graphite.

**Conclusions.** On the basis of the presented data we conclude that the $MoS_2$ particles in the sulfided catalyst are loosely connected to the alumina support, which is in agreement with earlier models for the Type-2 active phase. Due to this loose

interaction of the $MoS_2$ with the alumina support a network of pores smaller than 3 nm is created upon sulfidation, which was confirmed by nitrogen physisorption. The $MoS_2$ particles form a complex interconnected structure within the alumina support and occupy a substantial fraction of the mesopore volume. At the resolution obtained in this work the individual crystal planes of $MoS_2$ particles have been imaged, and the shapes of the resolved particles deviate largely from studies on model catalysts. A generalization of the presented results is not possible from our data and beyond the scope of this letter. The significance of the observation is limited to the described catalyst and provides a "proof of principle" for this new methodology. The presented results can be seen as a first measurement in a multivariant space relating preparation, activation, and test conditions with the actual 3D structure of the active catalyst. High-resolution electron tomography has delivered new fundamental insights into the structure of a complex catalyst and is expected to play a major role in the understanding and development of this important class of materials.

**Acknowledgment.** K.P.d.J. and H.F. acknowledge support by the National Research School Combination Catalysis. We thank Caroline van der Meij for TEM sample preparation and Hans Meeldijk for support with electron microscopy.

**Supporting Information Available:** Movies of the aligned HRTEM tilt series with an angular increment of 4° (Projections.qt), consecutive cross-sections through the reconstruction with 1 nm spacing between sections (Reconstruction.qt), and interconnected $MoS_2$ particles viewed at different rotations with an angular increment of 5° (Surface.qt). This material is available free of charge via the Internet at http://pubs.acs.org.

## References and Notes

(1) (a) Topsøe, H.; Clausen, B. S. *Catal. Rev. Sci. Eng.* **1984**, *26*, 395. (b) van Veen, J. A. R.; Gerkema, E.; van der Kraan, A. M.; Knoester, A. *J. Chem. Soc., Chem. Commun.* **1987**, *22*, 1684. (c) van Veen, J. A. R.; Colijn, H. A.; Hendriks, P. A. J. M.; van Welsenes, A. J. *Fuel Process. Technol.* **1993**, *35*, 137.

(2) (a) Dhas, N. A.; Ekhtiarzadeh, A.; Suslick, K. S. *J. Am. Chem. Soc.* **2001**, *123*, 8310. (b) Raybaud, P.; Hafner, J.; Kresse, G.; Toulhoat, H. *Phys. Rev. Lett.* **1998**, *80*, 1481. (c) Nørskov, J. K.; Clausen, B. S.; Topsøe, H. *Catal. Lett.* **1992**, *13*, 1. (d) Lauritsen, J. V.; Bollinger, M. V.; Lægsgaard, E.; Jacobsen, K. W.; Nørskov, J. K.; Clausen, B. S.; Topsøe, H.; Besenbacher, F. *J. Catal.* **2004**, *221*, 510. (e) Lauritsen, J. V.; Nyberg, M.; Nørskov, J. K.; Clausen, B. S.; Topsøe, H.; Lægsgaard, E.; Besenbacher, F. *J. Catal.* **2004**, *224*, 94.

(3) (a) Bouwens, S. M. A. M.; van Zon, F. B. M.; van Dijk, M. P.; van der Kraan, A. M.; de Beer, V. H. J.; van Veen, J. A. R.; Koningsberger, D. C. *J. Catal.* **1994**, *146*, 375. (b) Hensen, E. J. M.; de Beer, V. H. J.; van Veen, J. A. R.; van Santen, R. A. A *Catal. Lett.* **2002**, *84*, 59.

(4) (a) Chianelli, R. R.; Ruppert, A. F.; José-Yacamán, M.; Vázquez-Zavala, A. *Catal. Today* **1995**, *23*, 269. (b) Eijsbouts, S. *Appl. Catal., A* **1997**, *158*, 53. (c) Sun, M.; Nicosia, D.; Prins, R. *Catal. Today* **2003**, *86*, 173. (d) Shimada, H. *Catal. Today* **2003**, *86*, 17.

(5) (a) Srinivasan, S.; Datye, A. K.; Peden, C. H. F. *J. Catal.* **1992**, *137*, 513. (b) van Langefeld, A. D.; Stockmann, R. M.; Moulijn, J. A.; Zandbergen, H. W. *J. Mol. Catal. A: Chem.* **1995**, *102*, 147. (c) De la Rosa, M. P.; Texier, S.; Berhault, G.; Camacho, A.; José-Yacamán, M.; Mehta, A.; Fuentes, S.; Montoya, J. A.; Murrieta, F.; Chianelli, R. R. *J. Catal.* **2004**, *225*, 288.

(6) (a) Kürner, J.; Frangakis, A. S.; Baumeister W. *Science* **2005**, *307*, 436. (b) Grabenbauer, M.; Geerts, W. J. C.; Fernandez-Rodriguez, J.; Hoenger, A.; Koster, A. J.; Nilson, T. *Nat. Methods* **2005**, *2*, 857.

(7) Arslan, I.; Yates, T. J. V.; Browning, N. D.; Midgley, P. A. Science **2005**, *309*, 2195.

(8) (a) Janssen, A. H.; Koster, A. J.; de Jong, K. P. *Angew. Chem., Int. Ed.* **2001**, *40*, 1102. (b) Janssen, A. H.; Yang, C.-M.; Wang, Y.; Schüth, F.; Koster, A. J.; de Jong, K. P. *J. Phys. Chem. B* **2003**, *107*, 10552. (c) Midgley, P. A.; Weyland, M.; Thomas, J. M.; Johnson, B. F. G. *Chem. Commun.* **2001**, *10*, 907. (d) Thomas, J. M.; Midgley, P. A.; Gai, P. L.; Yates, T. J. V.; Weyland, M. *Microsc. Microanal.* **2004**, *10* (Suppl. 2), 34.

(9) (a) Anderson, M. W.; Ohsuna, T.; Sakamoto, Y.; Liu, Z.; Carlsson, A.; Terasaki, O. *Chem. Commun.* **2004**, *8*, 907. (b) Ziese, U.; de Jong, K. P.; Koster, A. J. *Appl. Catal., A* **2004**, *260*, 71. (c) Thomas, J. M.; Midgley, P. A. *Chem. Commun.* **2004**, *11*, 1253.

(10) Eijsbouts, S.; van den Oetelaar, L. C. A.; van Puijenbroek, R. R. *J. Catal.* **2005**, *229*, 352.

(11) (a) Kremer J. R.; Mastronarde D. N.; McIntosh J. R. *J. Struct. Biol.* **1996**, *116*, 71. (b) Mastronarde, D. N. *J. Struct. Biol.* **1997**, *120*, 343.